# Chapter 2

# Enhanced conductance near zero voltage bias in mesoscopic superconductor – semiconductor junctions.

We have studied the conductance enhancement near zero voltage bias of double barrier Nb – $p^{++}$Si – CE junctions, where we chose for the counter electrode CE either Nb, Al or W. The experiments show a large correction, $\Delta G \approx 0.1 G_{\mathrm{N}}$, on the classical superconductor – insulator – normal-metal (SIN) conductance. We present measurements of the temperature, magnetic field and voltage dependence, and we interpret the observed results within the available theoretical models for coherent Andreev reflection, as provided by several authors.

## 2.1 Introduction.

Superconductor semiconductor devices have become a topic of intensive research in recent years. They provide excellent systems to study transport phenomena in

super – normal-conductor (SN) structures. Due to the superconducting energy gap $\Delta$ non-linear effects in the conductance are already present at very low voltages. One of the most interesting phenomena that may occur at the interface between a superconductor and a normal metal is Andreev reflection [1]. An electron, with an energy $E < \Delta$, can only penetrate the superconductor by finding a matched electron, thus leaving a hole which is (retro-) reflected into the normal metal.

Blonder *et al.* [2] describe transport across a SIN interface in terms of Andreev and normal reflection, for arbitrary transparencies $\Gamma$ of the interface. In SIN, the I stands for a barrier at the interface, either due to a actual tunnel barrier, a Schottky barrier, or a Fermi-velocity mismatch between the two materials. The barrier strength is expressed with a dimensionless parameter $Z = H/\hbar v_F$, where $H$ is the strength of the $\delta$-function potential barrier at the interface. Octavio *et al.* [3] used this model to give an explanation for the subharmonic gap structures (SGS) in SNS junctions, in terms of multiple Andreev reflections, as originally proposed by Klapwijk *et al.* [4]. This (OTBK) model, with some simplifications made by Flensberg *et al.* [5], also explains the occurence of a current deficit or an excess current at higher voltages, depending on the barrier strength.

For double barrier SNS structures it is crucial to take into account phase coherent transport, especially for the description of the Josephson effect. Kastalsky *et al.* [6] reported experimental results that clearly indicate that phase coherence is also important for single SN junctions, in particular at low energies. They found an enhancement of the conductance of Nb – InGaAs contacts for low voltages, smaller than the superconducting energy gap $\Delta_{\mathrm{Nb}}$, at temperatures well below the superconducting transition temperature $T_c$ of Nb. The enhancement was of the order of $G_{\mathrm{N}}$, the normal state conductance, which is well beyond the small modifications usually given by quantum corrections to the conductance, e.g. due to weak localization [7]. They interpreted this effect by assuming a finite pair current across the SIN interface, using a superconducting proximity model proposed by Geshkenbein and Sokol [8],

based on the time-dependent Ginzburg-Landau theory for gapless superconductors.

An alternative model to explain the large conductance enhancement in terms of phase coherent electronic transport was given by Van Wees *et al.* [9], Marmorkos *et al.* [10], and Beenakker *et al.* [11, 12]. A disordered normal region, with an elastic mean free path $\ell$, is brought into contact with a superconductor, with a barrier present at the interface. The transparency of the barrier is taken to be much smaller than unity. In these models it is explicitely assumed that the pair potential in the normal metal $\Delta_{\rm N} = 0$. Because the normal region is assumed to be shorter than the phase breaking length $\ell_\phi$, coherent backscattering of electrons and holes causes multiple coherent Andreev reflections. A crucial aspect in these models is the phase conjugation at $E = E_{\rm F}$ and $B = 0$ in the Andreev reflection process, which is shown to result in an increase of the conductance at low bias. The magnitude of this effect can be calculated to be of order unity [9, 10, 11, 12], much larger than corrections due to weak localization, which are of the order $k_{\rm F}\ell$. In the paper by Marmorkos *et al.* [10] the limit where the barrier has a transparency $\Gamma$ close to 1 is also considered. In this case the opposite effect occurs, the conductance at low bias is reduced due to enhanced weak localization. This effect is again of the order $k_{\rm F}\ell$. Numerical studies on mesoscopic, superconductor – normal-metal structures have also been performed by Takane and Ebisawa [13, 14]. A similar model, using the quasi-classical Green's functions for non-equilibrium superconductors, is given by Zaitsev [15] and Volkov *et al.* [16, 17].

In this chapter a systematic experimental study of Nb – $p^{++}$Si – normal-metal junctions is presented. We varied both the junction length $L$ and the material of the normal metal counter electrode, in order to understand the observed deviations from the classical BTK-model.

## 2.2 Experimental setup and general results.

To study coherent backscattering in superconductor normal metal junctions, we need a system, where the normal metal is both disordered, with elastic mean free path $\ell$, and has a length $L$ shorter than the phase breaking length $\ell_\phi$ at the measurement temperature:

$$\ell < L < \ell_\phi \tag{2.1}$$

We used metallic $p^{++}$Si as the normal metal, and Nb as the superconductor. Our samples are based on Si-membranes. They are fabricated using a selective, anisotropic etchant, which stops at the high Boron (B) concentration ($8 \times 10^{19}$ cm$^{-3}$) defined by ion implantation [18]. Different membrane thicknesses can be defined using different B-implantation profiles. At the Nb-Si interface a barrier is present. This barrier can have two contributions: a Schottky barrier, which has a very thin and non-uniform depletion layer due to the high doping level, and a barrier as a result of Fermi velocity mismatch between the Nb and Si. At the high doping levels used in this system, the standard Schottky barrier theory is no longer valid, because the calculated depletion length becomes comparable to the separation of the B acceptor ions, so the continuum model breaks down. The barrier strength obtained from experiment, $Z \simeq 2$, is very close to the theoretical minimum as calculated from Fermi-velocity mismatch, $Z_{\min} = \sqrt{(1-r)^2/4r} \simeq 1.3$, where $r$ is the ratio of the Fermi-velocities in both materials. Following the analysis of Van Huffelen *et al.* [19], the elastic mean free path is estimated to be $\ell \simeq 5$ nm, where we used for the bulk resistivity at $4.2$ K a value of $\rho = (7.7 \pm 1.0) \times 10^{-4}\ \Omega$cm. For a schematic picture of the samples, and of the sample geometry, see Fig. 2.1. From previous experiments by Van Huffelen *et al.* [20, 19] we learned that the inelastic mean free path for electrons in the Si is much larger than the junction length, $\ell_{\rm in} \gg L (= 50$ nm$)$, as is clear from the high orders of multiple Andreev reflections. As a first approximation, in the absence of magnetic impurities, we can assume that

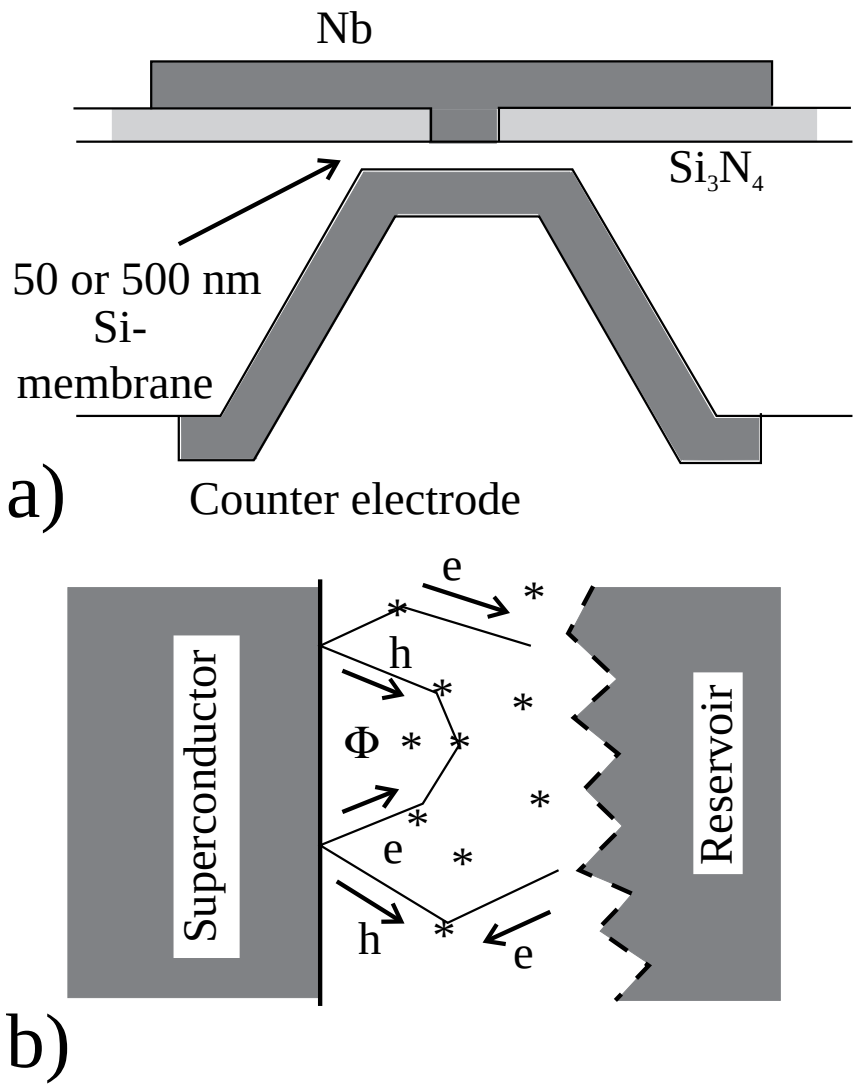


*Figure 2.1: Schematic picture of the junctions (a). A degenerately B-doped, Si-membrane ($n = 8 \times 10^{19}\mathrm{cm}^{-3}$), with $L = 500$ nm and two superconducting Nb-electrodes (sample* A*), or $L = 50$ nm and a normal metal counter electrode of Al (sample* B*) or W (sample* C*). Fig. (b) shows the geometry used in the model by Van Wees* et al. *[9], a superconductor in contact with a disordered normal conductor. For a detailed explanation see the text.*

the phase coherence length $\ell_\phi \simeq \ell_{\mathrm{in}}$.

We used three different samples, whose properties are listed in Table 2.1, together with some experimental results. The first type (sample *A*) are $500$ nm thick Si-

*Table 2.1: Basic sample properties*

| sample: | *A* | *B* | *C* |
|---|---|---|---|
| Counter Electrode | Nb | Al | W |
| $T_{c,CE}$ (K) | 9.2 | 1.18 | 0.015 |
| $L$ (nm) | 500 | 50 | 50 |
| Contact: | | | |
| area ($\mu$m$^2$) | 12 | 100 | 36 |
| $R_{c1}$ ($\Omega\mu$m$^2$)[a] | 5 | 300 | 540 |
| $R_{c2}$ ($\Omega\mu$m$^2$)[a] | 5 | 300 | 1620 |
| low voltage conductance peak | | | |
| $\Delta G/G\|_{V=0}$ (%) | 10 | 10 | 15 |
| width (mV) | 0.1 | 0.3 | 0.6 |
| lowest conductance ($\Omega^{-1}$)[b] | 0.34 | $9.85 \times 10^{-3}$ | $1.06 \times 10^{-2}$ |
| $G_{\rm N}/G\|_{V=0}$[c] | 5 | 1.7 | 1.5 |

[a] *$R_{c1,c2}$ is defined as the contact resistance multiplied by the contact area defined by lithography.*

[b] *The value of $dI/dV|_{V=0}$, without any conductance enhancement, is extrapolated from the tunnel curve (this is $(R_{\rm NS}^{\rm class})^{-1}$ from Ref. [12]).*

[c] *The depth of the tunnel dip, where $G_{\rm N}$ is the normal state conductance at $V > \Delta/e$, and $G|_{V=0}$ is the lowest conductance as extrapolated from the tunnel curve.*

membranes with Nb electrodes on both sides. Following the Kupriyanov-Lukichev theory [21], we expect the supercurrent in these junctions to be negligibly small. Typical measured curves are given in Fig. 2.2. A sharp peak near $V = 0$ in the differential conductance is observed. This is believed not to be a precursor of a supercurrent, since it does not exhibit a Fraunhofer diffraction pattern in the magnetic field dependence (not shown). At temperatures below $100$ mK the height of the conductance peak saturates, whereas for a true supercurrent it would increase

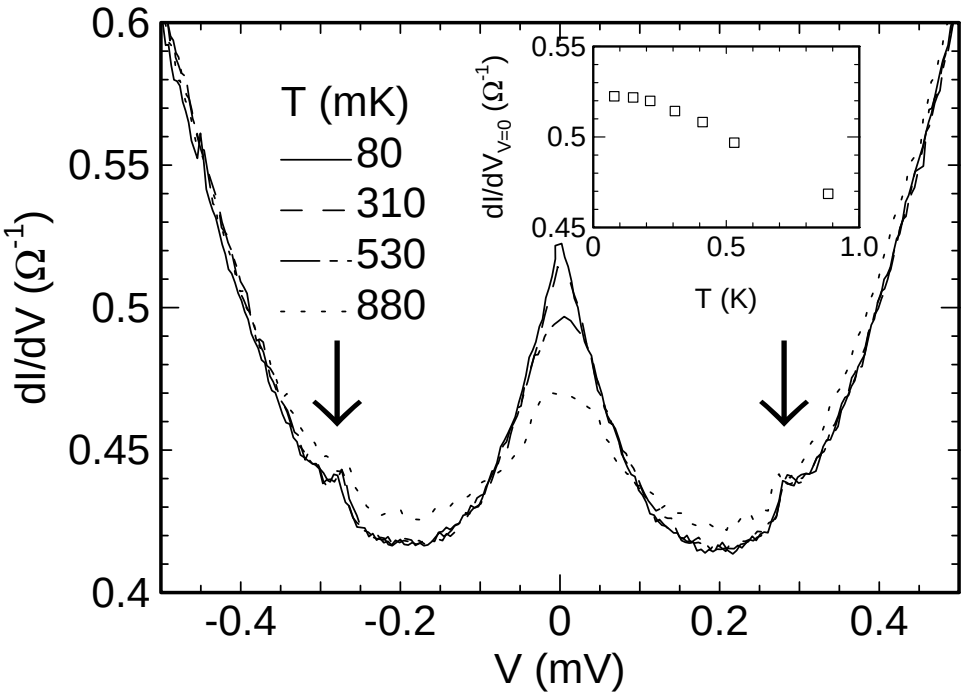


*Figure 2.2: Differential conductance as a function of voltage, for a thick membrane ($500$ nm), with two Nb electrodes, measured at $95$ mK. The arrow points to a small conductance peak at nonzero voltage, which appears in some samples. In the inset the temperature dependence of the zero voltage bias conductance is plotted, showing a saturation at low temperatures.*

to infinity (see the inset of Fig. 2.2). In some samples, a small feature can be seen at $V \simeq 0.28$ mV, as indicated by the arrows in Fig. 2.2. In most samples it is absent, and it is therefore believed to be an artefact, of unknown origin.

The conductance enhancement due to coherent backscattering is expected to be more prominent for $\ell_\phi \gg L$, and because it is uncertain whether $\ell_\phi > 500$ nm, we also studied thin ($50$ nm) membranes. For the superconducting top electrode we still used Nb, but we replaced the Nb of the bottom electrode by either Al (sample *B*), or W (sample *C*). Although Al becomes superconducting below $T_c = 1.18$ K, sample *B* did not show a supercurrent, presumably due to somewhat higher barriers at the Nb – Si and the Si – Al interfaces. These higher barriers are due to the fabrication,

and they are also present in sample *C*. Due to the presence of these barriers, the normal state resistance $R_{\mathrm{N}}$, at voltage $V > \Delta/e$, is higher.

The differential conductance of sample *B* is shown in Fig. 2.3, for different temperatures (a) and for different applied magnetic fields (b). Despite the lower conductance as a result of the barriers, the conductance enhancement at low voltage bias is of the same order as for sample *A*. As can be seen from Fig. 2.3(a), there is a saturation in the height of the conductance peak. When the temperature is decreased from $170\ \mathrm{mK}$ to $70\ \mathrm{mK}$, the peak height is not increased further. Analogous to the supercurrent in SNS junctions, the effect is expected to saturate when the coherence length $\xi(T) = \sqrt{\hbar D/kT}$ exceeds the junction length $L$. A further discusion will be given in section 2.3. In the inset of Fig. 2.3(a) the full curve up to voltages well above $\Delta_{\mathrm{Nb}}/e$ is given, for the lowest temperature ($70\ \mathrm{mK}$). It shows SIN tunneling behaviour due to the superconducting energy gap, except for the small peak around $V = 0$. From Fig. 2.3(b) one can see that on applying a magnetic field not only the zero voltage conductance peak is suppressed, but also the width of the tunnel dip is decreased. This last effect is a result of the magnetic field dependence of the superconducting energy gap, both of the Nb and the Al. The abrupt change in the tunnel characteristic from $100$ to $120\ \mathrm{mT}$ is a result of exceeding the critical field of the Al, which reduces the width of the tunnel dip from $\Delta_{\mathrm{Nb}} + \Delta_{\mathrm{Al}}$ to $\Delta_{\mathrm{Nb}}$. The tunnel dip appears broader than $\Delta_{\mathrm{Nb}}/e = 1.5\ \mathrm{mV}$ because of the high series resistance of the Si – Al interface.

Fig. 2.4 shows the differential conductance of sample *C*, Nb – Si – W, again for different temperatures (a) and applied magnetic fields (b). Although from Fig. 2.4(a) a saturation of the conductance enhancement is not clearly visible, it can not be excluded from the presented data. Saturation could very well take place somewhere within the temperature range of $195$ to $100\ \mathrm{mK}$. Another important notion that can be extracted from this figure is, that the temperature dependence of the enhanced conductance peak is not due to simple thermal smearing, averaging

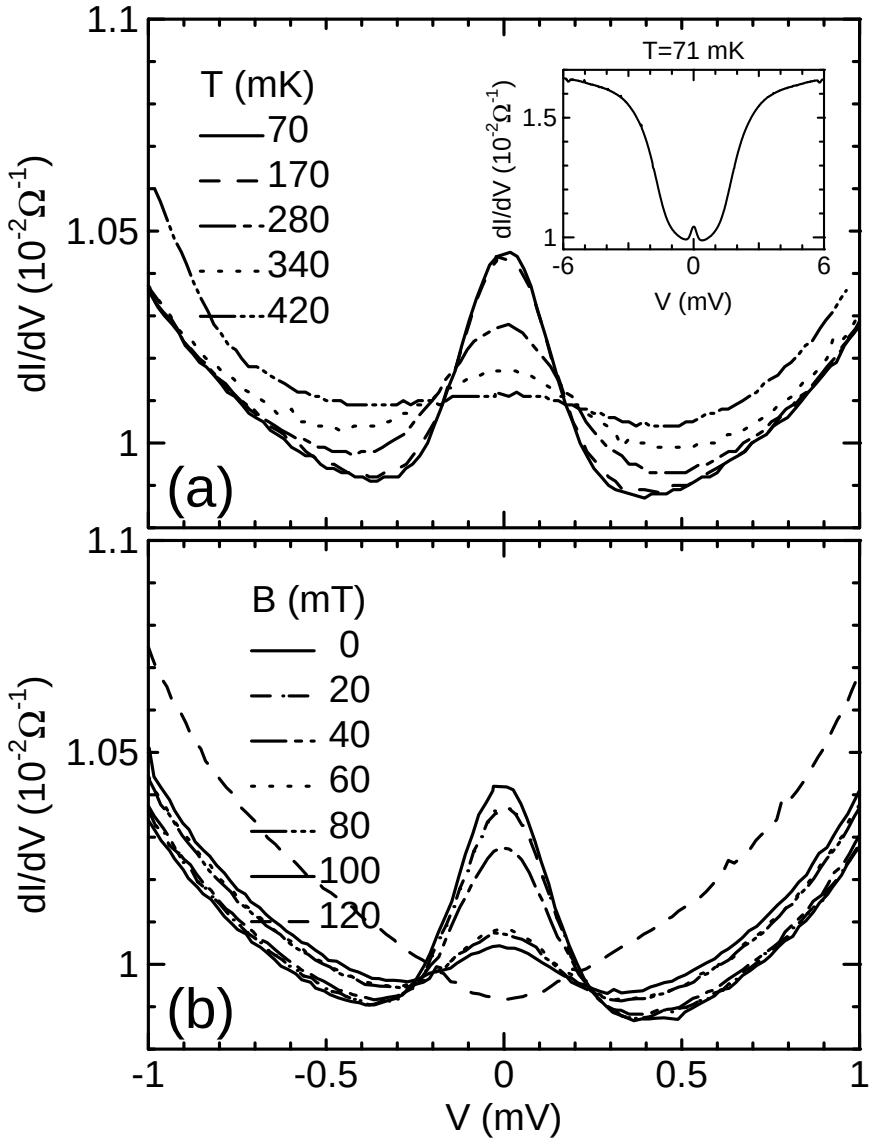


*Figure 2.3: Differential conductance as function of voltage, for a Nb – Si – Al junction, for various temperatures (a), and magnetic fields (b). The inset of (a) shows the overall conductance curve for the lowest temperature. In this inset the small peak at zero voltages can easily be identified as a small deviation from the normal tunnel curve. For this sample the contact hole in the $Si_3N_4$ layer is* $10 \times 10\ \mu\mathrm{m}^2$.

over a voltage range $k_{\mathrm{B}}T/e$. This would both lower and broaden the peak, whereas Fig. 2.4(a) only shows a decrease in height, the width remaining unchanged, or even

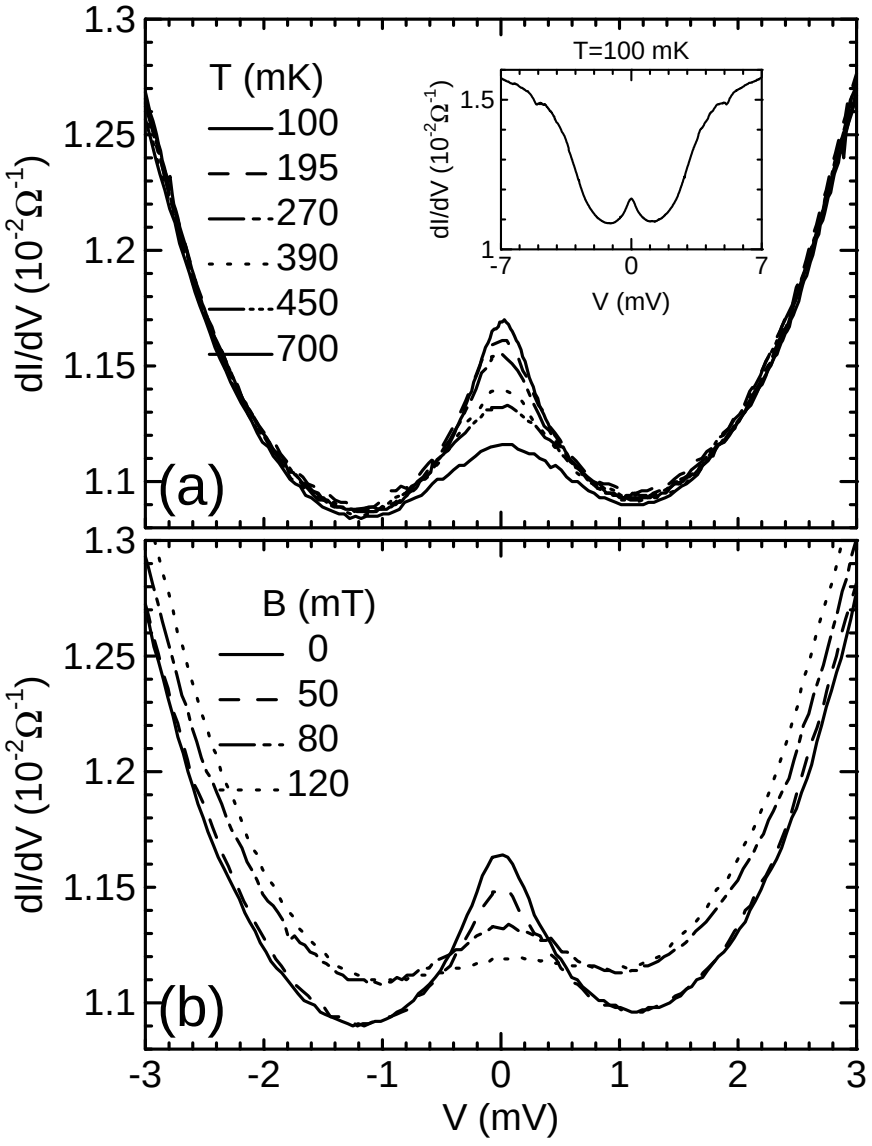


*Figure 2.4: Differential conductance as a function of voltage, for a Nb – Si – W junction, for various temperatures (a), and magnetic fields (b). The inset of (a) shows the overall conductance curve for the lowest temperature. For this sample the contact hole in the* $Si_3N_4$ *layer is* $6 \times 6\ \mu\mathrm{m}^2$.

slightly decreased. This phenomenon, which can also be seen in Fig. 2.2, is not yet understood. The dependence on a magnetic field, given in Fig 2.4(b), shows the same behaviour as for the Al sample (*B*). Both the zero voltage conductance peak

height, and the tunnel dip width are reduced with increasing magnetic field. The magnetic field that is needed to destroy the conductance enhancement is somewhat larger than for sample *B*. This is also true for the temperature and the voltage up to which the conductance enhancement is present. For this sample the Nb-Si interface has a barrier comparable to that of sample *B*, whereas the Si – W barrier is somewhat higher than the Si – Al barrier. Therefore a larger portion of the voltage drop occurs at this second barrier, and both the tunnel dip, and the conductance enhancement peak at low bias, appear broader. In all samples *A* – *C* the measured correction of the zero voltage conductance ($\Delta G/G|_{V=0}$), with respect to the BTK-model, is of the order 10 to 15%, which is a very large correction as compared to the small corrections in weak localization.

## 2.3 Comparison to theory.

Van Wees *et al.* [9], Marmorkos *et al.* [10] and Beenakker *et al.* [11, 12] describe the electronic transport in a disordered SIN structure (disordered N) using a scattering matrix formalism. A superconductor is brought into contact with a disordered semiconductor ($\ell, \xi < L$), with a low transparent barrier at the interface. The coherence length $\xi$ is the distance over which there is a correlation between electrons and holes in the semiconductor, as a result of Andreev reflections at the SIN interface. In general this coherence length $\xi = \xi(T)$ is temperature dependent. There is no pair potential induced in the normal region ($\Delta_{\rm N} = 0$), since it is assumed that electron-electron and electron-phonon interactions in the normal region are negligible. A further assumption of both models is that there are no inelastic scattering or phase breaking processes ($L \ll \ell_\phi$). Fig. 2.1(b) shows the path of an incoming electron, that can either be normal- or Andreev reflected at the SIN interface. If the electron is normal reflected, there is a good chance it will hit the SIN interface again after some path $\ell_{\rm path}$, having a second chance of being Andreev reflected. To calculate

the total Andreev reflection probability quantum interference between the hole wave functions formed in both events should be taken into account [9]. The total phase shift between both holes is given by:

$$\Delta\phi = \frac{2E\ell_{\rm path}}{\hbar v_{\rm F}} + 4\pi\frac{BA}{\Phi_0}, \tag{2.2}$$

where $A$ is the area enclosed by the path $\ell_{\rm path}$ and the superconductor, $B$ is the applied magnetic field. At $E = 0$ (measured with respect to $E_{\rm F}$) and $B = 0$ the phase shift $\Delta\phi = 0$, and the interference will be constructive and independent of path, and therefore result in an enhancement of the Andreev reflection probability. Coherent effects will be reduced if the average phase difference $\langle\Delta\phi\rangle$ is of the order of $2\pi$. Using $\langle\ell_{\rm path}\rangle \approx 0.35\ell/T_{\rm N}$ as the average path length, where $T_{\rm N} \approx \ell/L$ is the transmission probability of the middle region, and $\sqrt{\langle A^2\rangle} \approx 12\ell^2$ as the $\rm rms$ average area, we can therefore define [9] the critical voltage $eV_c = \frac{1}{2}h v_{\rm F}/\ell$ for which the enhanced conductance is suppressed. In an actual sample the single loop schematically shown in Fig. 2.1(b) can be extended to several loops, and in the particular case that $T_{\rm N} = 0.1$, the critical voltage $V_c$ is modified to $V_c^{\rm eff} \approx 0.05V_c$. Substituting the specific parameters of our samples: $eV_c^{\rm eff} \approx 2.9$ meV, and for the critical magnetic field $B_c = 0.042\Phi_0/\ell^2 = 6.9$ T. Obviously those numbers are much larger than the observed values. We therefore conclude that the average path length $\ell_{\rm path}$ and enclosed area $A$ are larger by an order of magnitude. Marmorkos *et al.* [10], who apply a more adequate description of impurity scattering than Van Wees *et al.* , also give expressions for the critical voltage and magnetic field. Again inserting the parameters of the Si we get: $eV_c = \frac{\pi}{2}\hbar v_{\rm F}\ell/L^2 \approx 0.29$ meV and $B_c = \Phi_0/LW \approx 20$ mT, where we used a junction length $L = 50$ nm, and a contact width $W = 4$ $\mu$m. The expression for the critical field $B_c$ however, is only valid for $W < L$. Furthermore we also need to take into account the penetration of the magnetic field into the superconductor. Inserting $L = 50$ nm $+ \lambda_{\rm London} = 100$ nm and $W = 400$ nm, which is a rough estimate of the average distance a particle travels along the interface before loosing its phase memory, we find $B_c \approx 100$ mT. This

value for $W$ is still large compared to the length $L$, but the very good agreement with the experiment suggests that this value is quite reasonable. If we compare the model of Marmorkos *et al.* [10] to sample *A*, Nb – $500\ \mathrm{nm}$ Si – Nb, we find much smaller values for $V_c$ and $B_c$ than from the experiment. This implies that the effective length $L^{\mathrm{eff}}$ for coherent effects is not the junction length $L = 500\ \mathrm{nm}$, but shorter. Comparing the height of the effect, Marmorkos *et al.* get a correction on the conductance $G_{\mathrm{NS}}|_{V=0}$ of the order unity. The experiments show a correction of 10 to 15%, which is only slightly smaller.

Recently Beenakker *et al.* [12] presented calculations on the (zero-voltage bias) resistance, for different lengths $L$ of the normal metal. The key result of their paper, for the transmission probability of the SIN interface $\Gamma \ll 1$, is given by:

$$\langle R_{\mathrm{NS}} \rangle = \frac{h}{2e^2 N} \frac{\ell}{L} \Gamma^{-2} \qquad \text{if } \Gamma L/\ell \ll 1 \tag{2.3}$$

$$\langle R_{\mathrm{NS}} \rangle = \frac{h}{2e^2 N} (\frac{L}{\ell} + \Gamma^{-1}) \qquad \text{if } \Gamma L/\ell \gg 1 \tag{2.4}$$

to be contrasted with the classical resistance (not taking into account phase coherent Andreev reflection)

$$R_{\mathrm{NS}}^{\mathrm{class}} = \frac{h}{2e^2 N} (\frac{L}{\ell} + 2\Gamma^{-2}) \tag{2.5}$$

where $N = A/(\frac{1}{2}\lambda_{\mathrm{F}})^2$ is the number of available modes. As a result of phase coherence of electrons and holes across the entire sample, the classical resistance $R_{\mathrm{NS}}^{\mathrm{class}}$ is, for $\Gamma L/\ell \gg 1$, modified to $\langle R_{\mathrm{NS}} \rangle$ as given in Eq.(2.4). As an example we will apply this model to sample *A*, Nb-$500\ \mathrm{nm}$-p$^{++}$Si-Nb. The advantage of sample *A* is that is has two almost identical interfaces, the $R_{\mathrm{NS}}$ of a single NS contact is thus simply the total resistance (at zero bias) divided by 2. From Fig. 2.2 we get (for the lowest temperature) $\langle R_{\mathrm{NS}} \rangle = 0.96\Omega$, and an interpolation of the tunnel curve gives $R_{\mathrm{NS}}^{\mathrm{class}} = 1.47\Omega$. Using $L/\ell = 100$, we get from the ratio $\langle R_{\mathrm{NS}} \rangle / R_{\mathrm{NS}}^{\mathrm{class}} = 0.653$ a value for $\Gamma = 0.18$. With Eq.(2.5) and (2.4) we calculate, using $\Gamma = 0.18$ and $N = \text{Contact Area}/(\frac{1}{2}\lambda_F)^2$, $R_{\mathrm{NS}}^{\mathrm{class}} = 0.97\Omega$ and $\langle R_{\mathrm{NS}} \rangle = 0.63\Omega$. The contact area in these samples is defined as $12\ \mu\mathrm{m}^2$, see also Table 2.1. These values are very

close to the experimental values, the small discrepancy being mainly due to the uncertainty of the effective contact area. According to this model the effect would be much stronger in the $50\ \mathrm{nm}$ samples, *B* and *C*, since the ratio $\langle R_{\mathrm{NS}}\rangle/R_{\mathrm{NS}}^{\mathrm{class}}$ is reduced significantly when $L/\ell$ is changed from 100 to 10, and $\Gamma = 0.18$ kept constant. In Fig. 2.3 and Fig. 2.4 the effect is shown to be of the same order as in sample *A*. A non-uniform interface, leading to a smaller effective contact area and on average a lower value of the interface transparency $\Gamma$, could account for a reduction of the conductance enhancement. A smaller effective contact area and $\Gamma$ also agrees with the larger contact resistance in samples *B* and *C*, see Table 2.1.

Calculations using quasi-classical Green's functions for non-equilibrium superconductors are given by Volkov *et al.* [16, 17]. Although the theoretical approaches are quite different, they yield qualitatively similar results. In some cases it has been verified that the two approaches also agree in detail (Marmorkos *et al.* [10]). Volkov *et al.* model a double barrier SININ′ structure, for which the current can be expressed as:

$$\begin{aligned} I &= \frac{1}{eR_N}\int_0^\infty \mathcal{D}(E)\mathcal{F}(E)\partial E \qquad (2.6)\\ \mathcal{D}(E) &= \frac{r_1+r_2+1}{\frac{r_1}{M_1(E)}+\frac{r_2}{M_2(E)}+\frac{1}{L}\int_0^L \frac{\partial x}{M_t(E,x)}}\\ \mathcal{F}(E) &= \frac{1}{2}\left[\tanh\left(\frac{E+eV}{kT}\right)-\tanh\left(\frac{E-eV}{kT}\right)\right] \end{aligned}$$

In Eq.(2.6) $\mathcal{D}(E)$ is the energy dependent transmission probability of the entire junction. In general the analytical expressions for $\mathcal{D}(E)$ are very complicated, however in certain limits, it is possible to calculate $\mathcal{D}(E)$ numerically. The ratio $r_{1,2}$ in Eq.(2.6) is defined as the barrier resistance $R_{1,2}$ over the bulk resistance $R$, where the normal state resistance $R_{\mathrm{N}} \equiv R_1 + R_2 + R$. The energy dependent function $M_1(E) = [\nu\nu_s + \eta\eta_s](x_1)$ at the SIN boundary, $x = x_1$, combines the normalized density of states in the superconductor S and the normal metal N. The function $M_2(E) = \nu(x_2)$ is determined by the density of states $\nu$ at the NIN′

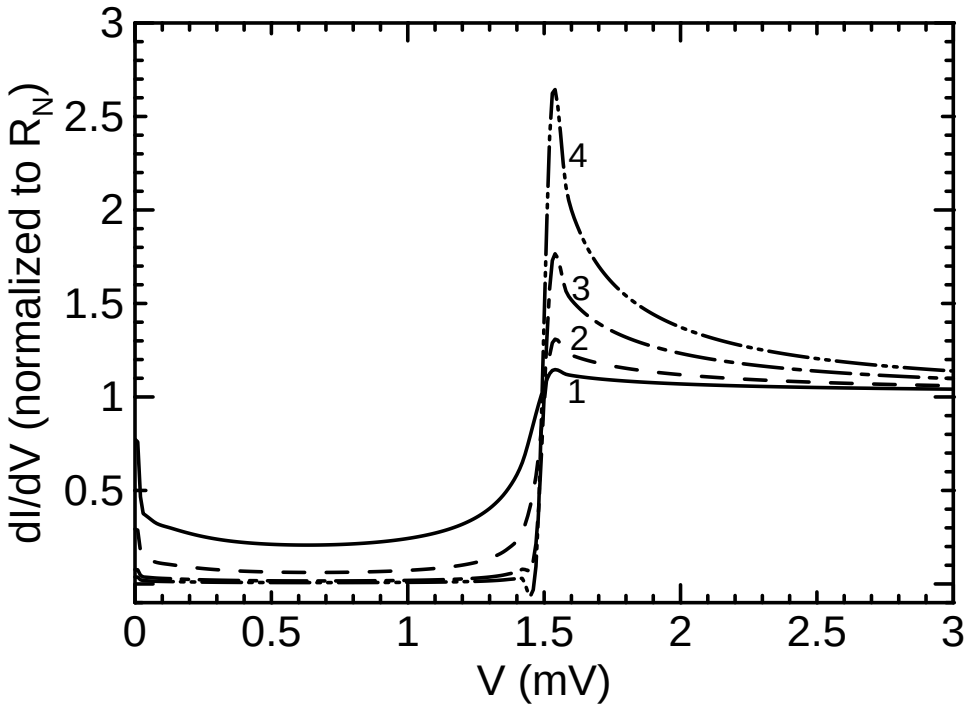


*Figure 2.5: Calculated normalized differential conductance as a function of applied voltage, according to the model by Volkov* et al. *[17].* $r_{1,2} = R_{1,2}/R$*, where* $R_{1,2}$ *is the interface resistance, and* $R$ *the resistance of the bulk. For the curves shown* $\Delta = 1.5$ meV*, and* $T = 100$ mK*. Values used for the different curves are, 1:* $r_1 = 5$, $r_2 = 35$, *2:* $r_1 = 10$, $r_2 = 30$, *3:* $r_1 = r_2 = 20$, *4:* $r_1 = 30$, $r_2 = 10$.

boundary, $x = x_2$, where it is assumed that the density of states in N′ is constant. In the middle N-layer $M_t(x) = \nu(x)^2 + \eta(x)^2$ is a combination of the two position dependent densities of states $\nu$ and $\eta$. The densities $\nu_s$ and $\eta_s$ are taken for BCS superconductors, whereas $\nu$ and $\eta$ have to be determined numerically from the exact boundary conditions(for details see Ref. [17]). Calculations for the low transparency limit ($r_1, r_2 \gg 1$), where the resistance of the middle layer can be neglected, are shown in Fig. 2.5. This limit is only valid for samples *B* and *C*, not for sample *A*, where the resistance of the bulk is not negligible. As can be seen there is a very good resemblance of the differential conductance curves obtained from the experiment.

From previous measurements [20, 19] it was already recognized that the Nb-Si

contact in our devices is highly non-uniform. Van Huffelen *et al.* had to assume a effective area of only 2 to 3% of the defined area, in order to get agreement between the calculated and measured normal state resistance. The ratios $r_{1,2}$ are defined as the contact resistance $R_{1,2}$ over the resistance $R$ of the middle region. For a uniform interface, the barrier resistance is directly proportional to its transparency, leading to a unique value for $r_{1,2}$, but since our barriers are non-uniform, it is not straight forward what values to choose for the ratios $r_1$ and $r_2$. This hinders an exact fit of the experiment, since in the model a uniform barrier is assumed at both interfaces.

## 2.4 Nb – 50 nm Si – Au junctions.

In the search for a good ohmic, non-superconducting, contact we also used Au contacts as the counter electrode CE. The Nb – Si – Au junctions, however, show completely different behavior from the samples *A* – *C* discussed above. Typical differential resistance curves are given in Fig. 2.6 as a function of temperature. Note that here the normalized differential resistance $(\partial V/\partial I)R_{\mathrm{N}}$ is plotted, instead of the conductance. At temperatures above $1.3\ \mathrm{K}$, upper panel of Fig. 2.6, a dip in the resistance, due to Andreev reflection, can be seen. The shape is however not as expected, first at an energy of $1.5\ \mathrm{meV}$ we see a small decrease in resistance, this corresponds to the superconducting energy gap $\Delta_{\mathrm{Nb}}$ of Nb. At lower energy, below approximately $0.5\ \mathrm{meV}$ a larger decrease in resistance is observed. Similar curves were also measured by Heslinga *et al.* [22], in Andreev reflection point-contact spectroscopy (ARPCS) measurements on Nb – Si interfaces, with low resistance, or large contact area, point-contacts. They claimed this dip at lower energy was the result of Andreev reflection from the induced gap $\Delta^0_{\mathrm{Si}}$. In smaller contacts they were even able to detect a double gap structure, both $\Delta_{\mathrm{Nb}}$ and $\Delta^0_{\mathrm{Si}}$. The presence of a double gap edge structure in the differential conductance was recently also predicted theoretically by Golubov and Kupriyanov [23], who studied a ballistic

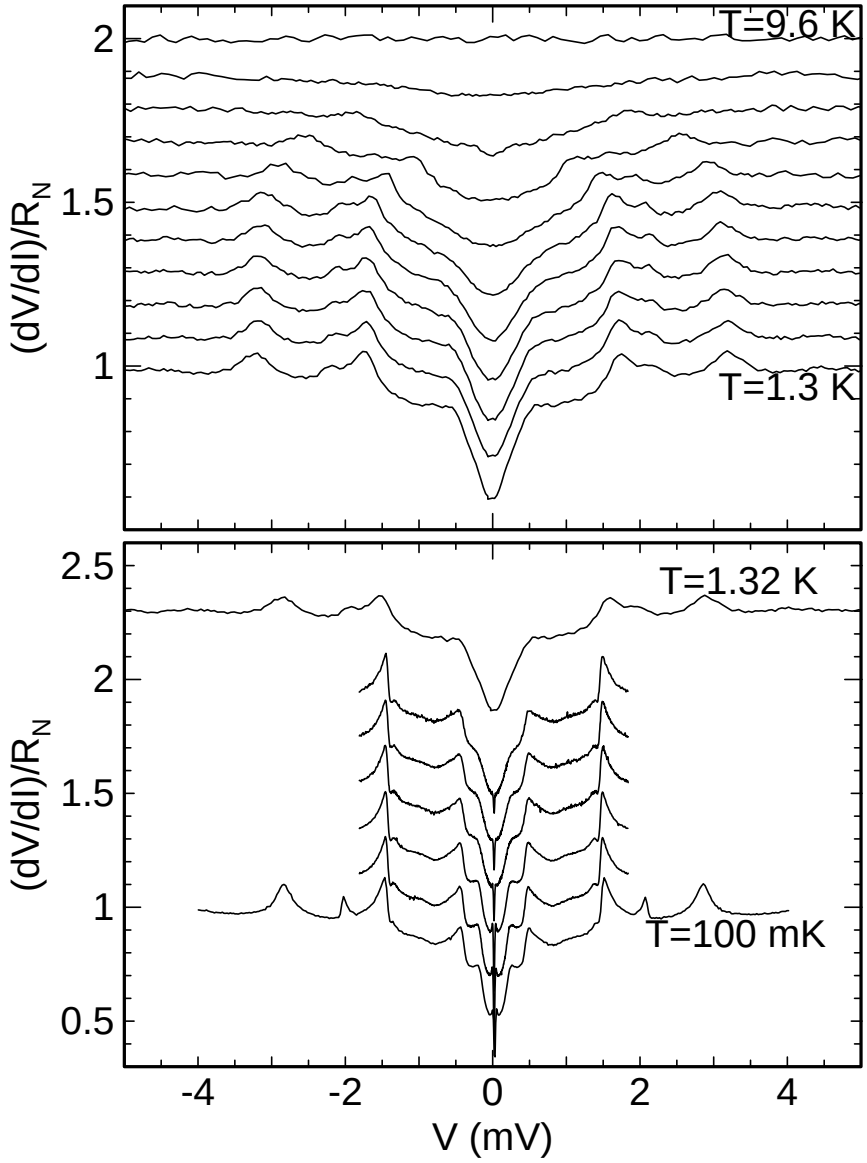


*Figure 2.6: Normalized differential resistance as a function of voltage, for a thin membrane ($50$ nm), with a Nb and a Au electrode, measured at different temperatures, curves are displaced by an offset for clarity. The upper panel shows data measured in a He-4 bath cryostat, curves in the lower panel are measured in a He-3/He-4 dilution refridgerator.*

NcS′S junction. Since we do not use a point-contact, but a large backside contact with a width $d_{\rm contact} \gg (\ell\ell_{\rm in}/3)^{1/2}$, it is unlikely that we will be able to observe a double gap structure in our junctions [24]. With increasing temperature the

central dip decreases, and $\Delta_{\rm Nb}$ is reduced to $0$ above the critical temperature $T_c = 9.2$ K, following the BCS dependence. At $T = 1.3$ K the zero voltage differential resistance $\partial V/\partial I|_{V=0} \approx 0.6 R_{\rm N}$, which implies almost perfect Andreev reflection. At low energy $eV < \Delta^0_{\rm Si}$ Andreev reflection takes place away from the Nb – Si interface, hence normal reflection is reduced to almost zero. For $V > \Delta_{\rm Nb}/e$ some resistance peaks of unknown origin, following the same (BCS-like) temperature dependence, are observed. Similar peaks, also following the BCS-gap as a function of temperature, were reported by Gao *et al.* [25], who measured Sn – GaAs/AlGaAs based SNS structures.

At low temperature, $T < 1.2$ K, the differential resistance curves are changed, see lower panel of Fig. 2.6. The peaks at high voltage, $V > \Delta_{\rm Nb}/e$ become sharper, which is the result of reduced thermal smearing at lower temperature. At approximately $0.2$ meV an extra feature starts to appear, and at zero voltage-bias a sharp dip in the resistance develops. From literature [26, 27] it is known that Si – Au alloys can become superconducting with critical temperatures ranging between $0.3$ and $2.25$ K. If we assume that due to alloying of the Au contact there is a $\rm Si_{1-x}Au_x$ alloy with a critical temperature $T_c' \approx 1.2$ K, we can explain the feature at $0.2$ meV as the superconducting energy gap $\Delta_{\rm Si_{1-x}Au_x}$ of the alloyed S′, and the sharp dip at $V = 0$ as a supercurrent in a SSmS′ junction. The magnetic field dependence is shown in Fig. 2.7. The energy gap of Nb, $\Delta_{\rm Nb}$, is reduced with increasing applied magnetic field, again following the BCS energy gap. The supercurrent is only reduced slightly, even at a field of $300$ mT, as can be seen from the small decrease of the zero voltage-bias dip. This weak magnetic field dependence suggests that the supercurrent flows in a small area of the junction, and that the superconducting Si – Au alloy is very inhomogeneous.

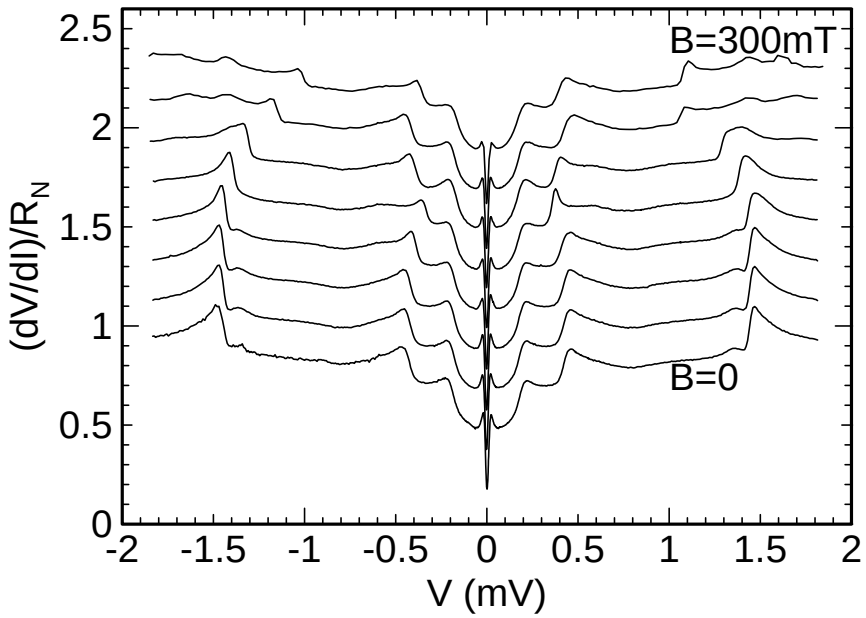


*Figure 2.7: Normalized differential resistance as a function of voltage, for a thin membrane (*$50\ \mathrm{nm}$*), with a Nb and a Au electrode, measured at different applied magnetic field, curves are displaced by an offset for clarity. All curves are measured at* $100\ \mathrm{mK}$.

## 2.5 Conclusions.

We have observed experimentally an enhancement of the conductance of Nb – $p^{++}$Si contacts, at low voltage bias ($eV \ll \Delta_{\mathrm{Nb}}$) and temperatures well below the superconducting transition temperature $T_c$ of Nb. Qualitatively we can explain our results with enhanced Andreev reflection due to multiple phase coherent reflections at the SSm interface, as proposed by Van Wees *et al.* [9]. A more quantitative comparison can be made by using the model of Beenakker and Marmorkos *et al.* [11, 10], who apply a more adequate description of impurity scattering. Using this model, together with the specific parameters of our samples, values for $V_c$ and $B_c$, the critical voltage and magnetic field above which the effect is diminished, are found to be in good agreement with the experiment. Regarding the amplitude of the corrections, Beenakker *et al.* [12] calculate the zero-voltage bias resistance as a function of the transmission probability $\Gamma$ of the SN interface, for different lengths

$L$ of the normal region. These calculations are in good comparison with sample *A* (Nb – $500$ nmSi – Nb), but predict larger corrections for samples *B* and *C* (Nb – $50$ nmSi – Al or W) than obtained from the experiment.

A different theoretical approach, using Green's function techniques, is used by Zaitsev [15] and Volkov *et al.* [16, 17]. Even though our samples have very inhomogeneous barriers at the interface, the resemblence of calculated curves to the experimental data is striking.

Discrepancies between theory and experiment cannot be resolved conclusively by the present experiment in view of the inhomogeneity of the interface. It is therefore essential, to study the influence of the shape of the interface barriers, on the electronic properties of these systems.

In Nb – Si – Au junctions we observed a large reduction in differential resistance as a result of Andreev reflection at the induced energy gap $\Delta^0_{\mathrm{Si}}$. At low temperature, $T < 1.2$ K, we also observed a feature at $0.2$ meV which we tentatively attribute to the superconducting energy gap of a $\mathrm{Si}_{1-x}\mathrm{Au}_x$ alloy with a critical temperature $T_c \approx 1.2$ K. The existence of this superconducting alloy is also suggested by the observation of a supercurrent at zero voltage-bias.

# References

[1] A. F. Andreev. *Zh. Eksp. Teor. Fiz.*, 46:1823, 1964. [Sov.Phys. JETP 19, 1228 (1964)].

[2] G. E. Blonder, M. Tinkham, and T. M. Klapwijk. *Phys. Rev. B*, 25:4515, 1982.

[3] M. Octavio, M. Tinkham, G. E. Blonder, and T. M. Klapwijk. *Phys. Rev. B*, 27:6739, 1983.

[4] T. M. Klapwijk, G. E. Blonder, and M. Tinkham. *Physica B&C*, 109&110B:1657, 1982.

[5] K. Flensberg, J. B. Hansen, and M. Octavio. *Phys. Rev. B*, 38:8707, 1988.

[6] A. Kastalsky, A. W. Kleinsasser, L. H. Greene, R. Bhat, F. P. Milliken, and J. P. Harbison. *Phys. Rev. Lett.*, 67:3026, 1991.

[7] G. Bergmann. *Phys. Reports*, 107:1, 1984.

[8] V. B. Geshkenbein and A. V. Sokol. *Zh. Eksp. Teor. Fiz.*, 94:259, 1988. [Sov. Phys. JETP 67, 362 (1988)].

[9] B. J. van Wees, P. de Vries, P. Magnée, and T. M. Klapwijk. *Phys. Rev. Lett.*, 69:510, 1992.

[10] I. K. Marmorkos, C. W. J. Beenakker, and R. A. Jalabert. *Phys. Rev. B*, 48:2811, 1993.

[11] C. W. J. Beenakker. *Phys. Rev. B*, 46:12841, 1992.

[12] C. W. J. Beenakker, B. Rejaei, and J. A. Melsen. *Phys. Rev. Lett.*, 72:2470, 1994.

[13] Y. Takane and H. Ebisawa. *J. Phys. Soc. Jpn.*, 61:2858, 1992.

[14] Y. Takane and H. Ebisawa. *J. Phys. Soc. Jpn.*, 61:1685, 1992.

[15] A. V. Zaitsev. *Pis'ma Zh. Eksp. Teor. Fiz.*, 51:35, 1990. [JETP Lett., 51, 41 (1990)].

[16] A. F. Volkov and T. M. Klapwijk. *Phys. Lett. A*, 168:217, 1992.

[17] A. F. Volkov, A. V. Zaitsev, and T. M. Klapwijk. *Physica C*, 210:21, 1993.

[18] W. M. van Huffelen, M. J. de Boer, and T. M. Klapwijk. *Appl. Phys. Lett.*, 58:2438, 1991.

[19] W. M. van Huffelen, T. M. Klapwijk, D. R. Heslinga, M. J. de Boer, and N. van der Post. *Phys. Rev. B*, 47:5170, 1993.

[20] W. M. van Huffelen, T. M. Klapwijk, and L. de Lange. *Phys. Rev. B*, 45:535, 1992.

[21] M. Y. Kupriyanov and V. F. Lukichev. *Zh. Eksp. Teor. Fiz.*, 94:139, 1988. [Sov. Phys. JETP 67, 1163 (1988)].

[22] D. R. Heslinga, S. E. Shafranjuk, H. van Kempen, and T. M. Klapwijk. *Phys. Rev. B*, 49:10484, 1994.

[23] A. A. Golubov and M. Y. Kupriyanov. *Pis'ma Zh. Eksp. Teor. Fiz.*, 61:830, 1995. [JETP Lett. **61**, 851 (1995)].

[24] A. G. M. Jansen, A. P. van Gelder, and P. Wyder. *J. Phys. C*, 13:6073, 1980.

[25] J. R. Gao, J. P. Heida, B. J. van Wees, T. M. Klapwijk, G. Borghs, and C. T. Foxon. *Surface Science*, 305:470, 1994.

[26] D. Moeckel. *INIS Atomindex*, 8:Abstr. No. 339345, 1977.

[27] T. Furubayashi, N. Nishida, M. Yamaguchi, K. Morigaki, and H. Ishimoto. *Solid State Comm.*, 58:587, 1986.